Flame ignition and extinction modelling using infinitely fast chemistry in large eddy simulations of fire-related reacting flows

Georgios Maragkos[*], Alexander Snegirev, Jeri At Thabari, Bart Merci

Department of Structural Engineering and Building Materials, Ghent University, Technologiepark-Zwijnaarde 60, 9052 Zwijnaarde, Belgium.

*Corresponding author. Email: Georgios.Maragkos@UGent.be

Highlights:

- LES results focusing on flame ignition and extinction modelling are presented.
- A dynamic approach for turbulence, combustion and radiation modelling is employed.
- The ignition and extinction criteria consider the local properties of the flow.
- The results are fairly grid insensitive and agree well with the experiments.

Abstract:

Large eddy simulations with the use of infinitely fast chemistry, focusing on flame ignition and extinction modelling, are presented within the context of fires. A dynamic approach with respect to turbulence, combustion and radiation modelling is employed in the simulations. Flame ignition is modelled based on an ignition temperature, which varies with the local sub-grid scale strain rate, while flame extinction is modeled based on the concept of a critical flame temperature, which varies with the local mixing time scale. Validation of the approach is made by considering four different experiments, involving both no-extinction and extinction scenarios. Focus is put on the predictive capabilities of the simulations, with respect to different grid sizes, by comparison to experimental data involving both first and second order statistics, and data available in the literature for different grid sizes and for the different fuels considered. The predicted flame temperatures and combustion efficiencies with the proposed approach agree fairly well, both qualitatively and quantitatively, with the experiments and data for the limiting oxygen concentration from the literature.

Keywords: ignition; extinction; LOC; combustion; fire; LES;

1. Introduction

Flame extinction is an important physical and chemical process that has received much attention in the past within the context of fire safety engineering (i.e., considering the protection of material properties and the safety of human lives). Modelling of flame extinction with the use of Computational Fluid Dynamics (CFD) with infinitely fast chemistry, which is currently the state-of-the-art approach for combustion modelling in Large Eddy Simulations (LES) of fires, still remains challenging, though. The difficulties do not only lie in the interconnecting nature of the various processes that need to be modelled (e.g., related to turbulence, combustion and radiative heat transfer among others) but also in the fact that accurate numerical predictions are required over a wide range of length scales.

40　Many CFD codes (e.g., FDS, FireFOAM) used for simulations of fire scenarios often rely on the
41　concept of either a critical flame temperature (CFT) (e.g., [1], [2], [3]) or a critical Damköhler
42　number (e.g., [4], [5], [6], [7], [8]) to model flame extinction. Depending on the fuel, the CFT is
43　typically assigned a constant value in the range of 1450 - 1780 K [9] (a value of 1600 K [1] can be
44　considered representative for many typical hydrocarbon fuels). Flame (re-)ignition has mainly
45　been modelled considering a constant temperature with combustion allowed to proceed if the
46　temperature of an initially suppressed mixture in a grid cell exceeds an a priori prescribed value
47　(i.e., either set to the auto-ignition temperature (AIT) of the fuel [1], or to a constant value (e.g.,
48　1000 K [5] - 1100 K [6]).

49　The work presented here reports on LES, using infinitely fast chemistry, and focuses on flame
50　ignition using an ignition temperature, which varies with the local sub-grid scale (sgs) strain rate,
51　while flame extinction modelling is based on the concept of a critical flame temperature, which
52　varies with the local mixing time scale. A dynamic approach with respect to turbulence (i.e.,
53　dynamic turbulence model parameters and turbulent Prandtl number), combustion (i.e., sgs mixing
54　model not involving any tuning parameters) and radiation (i.e., prediction of the radiative fraction
55　with an emission correction term for coarse grids) modelling is employed in the simulations. The
56　focus is put on the predictive capabilities of the numerical simulations with respect to different
57　grid sizes ranging from coarser (i.e., typically applied for engineering type of calculations) to finer
58　ones (i.e., in the order of 1 cm or less), which are typically required for accurate LES of buoyant
59　turbulent diffusion flames.

60　Validation of the simulations is made through comparison to four experimental test cases from the
61　MaCFP workshop series [10]. The scenarios involve buoyancy-driven flows, including both no-
62　extinction and extinction cases, and consider different burner geometries, fuels and fire sizes of
63　different levels of complexity. The cases involve quenching due to dilution, which is one of the
64　mechanisms of flame extinction, along with thermal quenching, which typically occurs in fires.
65　The scenarios considered for validation include: McCaffrey's fire plume experiments involving a
66　30 cm square burner with natural gas and heat release rates of 14.4 - 57.5 kW [11]; NIST's 1 m in
67　diameter methanol pool fire experiments with a heat release rate of 256 kW [12]; UMD's line
68　burner [13] (5 cm wide by 50 cm long) experiments involving a methane diffusion flame of 50 kW
69　with the co-flowing air issued at 85 g/s and with a decreasing oxygen concentration until extinction
70　occurs; and FM Global's experiments [14] involving a 15 cm in diameter burner involving an
71　ethylene 15 kW fire with a co-flowing air issued with a velocity of 0.041 m/s. The extinction cases
72　of the FM Global burner involve 10 kW methane, propane, propene and ethylene fires with the
73　oxygen concentration in the co-flow slowly reduced until extinction occurs. The combination of
74　these experimental test cases provides a wealth of experimental data, involving both first and
75　second order statistics, useful for CFD model validation. A more detailed description of the cases
76　considered can be found in https://github.com/MaCFP/macfp-db.

2. Numerical modelling

78　The CFD code FireFOAM, developed by FM Global, is used for numerical modelling. An
79　overview of the governing equations and the various sub-models employed is given below [15]:

$$\frac{\partial \bar{\rho}}{\partial t} + \nabla \cdot (\bar{\rho}\tilde{u}) = 0 \tag{1}$$

$$\frac{\partial (\bar{\rho}\tilde{u})}{\partial t} + \nabla \cdot (\bar{\rho}\tilde{u}\tilde{u}) = -\nabla \bar{p} + \nabla \cdot \left[\mu_{eff} \left(\nabla \tilde{u} + (\nabla \tilde{u})^T - \frac{2}{3}(\nabla \cdot \tilde{u})I \right) \right] + \bar{\rho}g \tag{2}$$

$$82 \qquad \frac{\partial(\bar{\rho}\tilde{Y}_k)}{\partial t} + \nabla \cdot \left(\bar{\rho}\tilde{u}\tilde{Y}_k\right) = \nabla \cdot \left[\bar{\rho}\left(D_{th} + \frac{\nu_{sgs}}{Pr_t}\right)\nabla\tilde{Y}_k\right] + \bar{\dot{\omega}}_k''' \qquad (3)$$

$$83 \qquad \frac{\partial(\bar{\rho}\tilde{h}_s)}{\partial t} + \nabla \cdot \left(\bar{\rho}\tilde{u}\tilde{h}_s\right) = \frac{D\bar{p}}{Dt} + \nabla \cdot \left[\bar{\rho}\left(D_{th} + \frac{\nu_{sgs}}{Pr_t}\right)\nabla\tilde{h}_s\right] - \nabla \cdot \bar{\dot{q}}_r'' + \bar{\dot{q}}_c''' \qquad (4)$$

84   where $\bar{\rho}$ is the density, $\tilde{u}$ is the velocity, $\bar{p}$ is the pressure, $\mu_{eff} = \mu + \mu_{sgs}$ is the effective
85   (molecular plus sgs) dynamic viscosity, I is the identity tensor, g is the gravitational acceleration,
86      $\tilde{Y}_k$ is the species mass fraction, D_{th} is the thermal diffusivity, Pr_t is the turbulent Prandtl number,
87      $\bar{\dot{\omega}}_k'''$ is the species reaction rate, $\tilde{h}_s$ is the sensible enthalpy, $\bar{\dot{q}}_r''$ is the radiative heat flux and $\bar{\dot{q}}_c''' =$
88      $-\bar{\dot{\omega}}_F'''\Delta H_c$ is the heat release per unit volume due to combustion with ΔH_c the heat of combustion
89   of the fuel. The code ignores differential diffusion, considers a unity Lewis number and $Sc_t = Pr_t$.

90   **2.1 Turbulence**

91   The dynamic Smagorinsky model is used for turbulence calculating the sgs viscosity as [16]:

$$92 \qquad \mu_{sgs} = \bar{\rho}(c_s\Delta)^2|\tilde{S}| \qquad (5)$$

93   where Δ is the filter size (i.e., cube root of the cell volume) and $\tilde{S}$ is the resolved strain rate.

94   The sgs kinetic energy is estimated as [17]:

$$95 \qquad k_{sgs} = c_I\Delta^2|\tilde{S}|^2 \qquad (7)$$

96   The model parameters c_s and c_I (as well as the turbulent Prandtl number, Pr_t) are calculated
97   dynamically based on a procedure previously outlined in [15].

98   The sgs dissipation rate is calculated as [17]:

$$99 \qquad \varepsilon_{sgs} = \frac{c_\varepsilon k_{sgs}^{3/2}}{\Delta} \qquad (8)$$

100   where the model parameter c_ε is calculated dynamically as [18]:

$$101 \qquad c_\varepsilon = \frac{(\mu+\mu_{sgs})\widehat{\Delta}\left[\frac{\partial\widehat{\tilde{u}_J}}{\partial x_i}\frac{\partial\widehat{\tilde{u}_J}}{\partial x_i}-\frac{\partial}{\partial x_i}\left(\frac{\widehat{\bar{\rho}\tilde{u}_J}}{\widehat{\bar{\rho}}}\right)\frac{\partial}{\partial x_i}\left(\frac{\widehat{\bar{\rho}\tilde{u}_J}}{\widehat{\bar{\rho}}}\right)\right]}{\bar{\rho}\left(\frac{\widehat{\bar{\rho}\tilde{u}_k\tilde{u}_k}}{2\widehat{\bar{\rho}}}-\frac{\widehat{\bar{\rho}\tilde{u}_k}}{2\widehat{\bar{\rho}}}\frac{\widehat{\bar{\rho}\tilde{u}_k}}{\widehat{\bar{\rho}}}\right)^{\frac{3}{2}}} \qquad (9)$$

102   with the hat denoting a top-hat filter (i.e., set to $\sqrt{6}$ times the filter size [15]).

103   **2.2 Combustion**

104   Combustion is considered to be infinitely fast, described by a one-step chemical reaction, with
105   turbulence-chemistry interactions modelled with the Eddy Dissipation Model (EDM). Within the
106   EDM, the fuel consumption rate is calculated as [19]:

$$107 \qquad \bar{\dot{\omega}}_F''' = -\bar{\rho}\frac{\min(\tilde{Y}_F,\ \tilde{Y}_{O_2}/s)}{\tau_{mix}} \qquad (10)$$

108   where $\tilde{Y}_F$ and $\tilde{Y}_{O_2}$ are the resolved fuel and oxygen mass fraction, respectively, and s is the
109   stoichiometric oxygen-to-fuel mass ratio.

110   The mixing time scale, τ_{mix}, is calculated as:

$$\tau_{mix} = \min(\tau_{lam}, \tau_{turb}) \tag{11}$$

112   which effectively considers mixing under laminar and turbulent conditions, respectively.

113   The laminar time scale is calculated as:

$$\tau_{lam} = \frac{\Delta^2}{D_{th}} \tag{12}$$

115   Considering that mixing can occur over a wide range of time scales, two of the most important
116   turbulent time scales are considered; the sub-grid scale velocity stretching time scale ($\tau_{stretch} =$
117   Δ/u'), associated with large-scale fluctuations and mixing, and the Kolmogorov time scale ($\tau_K =$
118     $(v/\epsilon_{sgs})^{1/2}$) associated with the mixing at the smallest turbulent scales (i.e., at molecular level).
119   The turbulent mixing time scale, τ_{turb}, is then calculated based on their geometric mean as [20]:

$$\tau_{turb} = \sqrt{\frac{\Delta}{u'}\left(\frac{v}{\epsilon_{sgs}}\right)^{\frac{1}{2}}} \tag{13}$$

121   where $u' = \sqrt{\frac{2k_{sgs}}{3}}$ is the rms of sgs turbulent velocity fluctuations.

2.3 Radiation

123   Radiation modelling considers the radiation intensity to be a function of spatial location and
124   angular direction and is obtained by solving the radiative transfer equation by the finite volume
125   discrete ordinates method. Absorption is considered through the weighted-sum-of-gray-gases
126   (WSGG) model [22]. Within WSGG, the total emissivity of a H_2O and CO_2 mixture is calculated
127   as the sum of fictitious gray gases weighted with a temperature dependent weighing factor as:

$$\varepsilon = \sum_{i=0}^{N_g} a_i(1 - e^{-\kappa_i pL}) \tag{14}$$

129   where N_g is the number of gray gases, a_i is the emissivity weighting factor of the ith gray gas, κ_i
130   is the absorption coefficient of the ith gray gas, p is the sum of the partial pressures of all absorbing
131   gases and L is the path length. In this case, four fictitious gray gases are used ($N_g = 4$), together
132   with a transparent gas ($i = 0$) representing the spectral windows between the absorption bands.

133   The weight factors, a_i, are calculated as a polynomial function of temperature as:

$$a_i = \sum_{j=0}^{4} b_{i,j} \tilde{T}^j, \qquad i > 0 \tag{15}$$

135   where $b_{i,j}$ are polynomial coefficients of the ith gray gas of the jth order. The emissivity weighting
136   factor for the transparent gas ($i = 0$) is calculated based on energy conservation: $a_0 = 1 - \sum_{i=1}^{N_g} a_i$.

137   The WSGG model coefficients can be obtained for different fuels by fitting Eq. (14) to line-by-
138   line (LBL)-based emissivity databases for different pL values. In this case, the coefficients needed
139   for the calculation $b_{i,j}$ and κ_i are taken from [23] for gas mixtures of H_2O and CO_2 with molar
140   fraction ratio equal to $M_r = p_{H_2O}/p_{CO_2} = 2$, representing typical products of methane combustion.

141　The total absorption coefficient, κ, is then calculated as:

$$\kappa = -\frac{ln(1-\varepsilon)}{L} \tag{16}$$

143　The path length, L, is calculated as:

$$L = 3.6\frac{V}{A} \tag{17}$$

145　where V and A are the volume and surface area, respectively, of the medium participating in the
146　absorption. A dynamic approach is employed for estimating L in which the volume of the medium
147　is calculated by summing all the cell volumes where reaction takes place (i.e., $\bar{\dot{q}}_c''' > 100\frac{kW}{m^3}$), and
148　by assuming a certain flame shape (e.g., conical or rectangular depending on the burner geometry),
149　the corresponding surface area is obtained.

150　Finally, the radiative heat fluxes in Eq. (4) are calculated as:

$$-\nabla \cdot \bar{\dot{q}}_r'' = \kappa G - \left(4\kappa\sigma\tilde{T}^4 + E\bar{\dot{q}}_c'''\right) = -\nabla \cdot \bar{\dot{q}}_r''^{,*} - E\bar{\dot{q}}_c''' \tag{18}$$

152　where σ is the Stefan-Boltzmann constant, G is the total irradiance and E is a correction in the
153　emission term calculated as:

$$E = \max\left(\chi_{r,exp.} - \frac{\iint_A \bar{\dot{q}}_r''^{,*}dA}{\iiint_V \bar{\dot{q}}_c'''dV}, 0\right) \tag{19}$$

155　where $\chi_{r,exp.}$ is the radiative fraction of the fuel, which is defined a priori based on experimental
156　data. The second term in Eq. (19), represents the predicted (simulated) radiative fraction, which is
157　calculated as the ratio of the heat reaching surface area, A, on the domain boundary by radiation,
158　to the total heat release rate inside the volume, V, of the computational domain. With the current
159　approach, absorption is considered everywhere in the domain (i.e., in both the flame and the plume
160　regions) even if the flame is under-resolved by the grid size. The correction by Eq. (19) is applied
161　to correct the emission source term, which tends to be under-predicted in the simulations with
162　coarse grids, particularly in the flame region, or when soot modelling is not modelled (which was
163　the case here in order to avoid added complexity). For cases involving flame extinction, $\chi_{r,exp.}$ is
164　not a constant value, but varies as a function of the oxygen concentration in the co-flow, according
165　to experimentally reported values for the test case considered.

166　**2.4 Flame ignition / extinction**

167　Flame ignition is an important modelling aspect because, if not considered properly, it can lead to
168　spurious (re-)ignition phenomena further downstream from the fire source. In this case, no flame
169　extinction is allowed if the cell temperature is equal or higher than the ignition temperature, T_{ign}:

$$\tilde{T} \geq T_{ign} \tag{20}$$

171　The main mechanisms for flame (re-)ignition are expected to be due to premixed auto-ignition
172　(controlled by chemistry) and non-premixed auto-ignition (controlled by mixing and chemistry)
173　which have been reported to require a temperature of approximately 1000 K [25]. In this work, the
174　required temperatures for ignition, T_{ign}, are taken from experimental data of non-premixed,
175　counterflowing jets of nitrogen-diluted fuels versus hot air [26, 27] for strain rates higher than 100
176　s⁻¹. The T_{ign} values for zero strain rates were considered to be the corresponding auto-ignition

177 temperatures of each fuel [9]. The ignition temperatures, T_{ign}, were then fitted using a third order
178 polynomial of the following form:

179 $$T_{ign, \, fuel} = aS_{sgs}^3 + bS_{sgs}^2 + cS_{sgs} + d \quad \text{for} \quad S_{sgs} \leq 300 \, s^{-1} \tag{21}$$

180 with the parameters a, b, c and d reported in Table 1.

181

182 Table 1. Parameters used in Eq. (23) for calculating T_{ign} for different fuels.

Fuel data	a	b	c	d
CH_4	6e-5	-0.0347	6.5893	813
C_3H_8	4e-5	-0.0286	6.7684	723
C_2H_6*	4e-5	-0.0279	5.9416	788

183 * Data used in the simulations when C_2H_4 or C_3H_6 is the fuel.

184 Considering that combustion is unresolved on the CFD grid (i.e., occurs on a sgs level), T_{ign} is
185 chosen to vary with the local sgs strain rate. The choice of a characteristic eddy strain rate is not
186 always straightforward to evaluate and different approaches have been suggested in the literature.
187 More specifically, a flame-stretching strain rate for buoyancy-induced turbulent flows, based on
188 the energy cascade theory, has been suggested by Yu et al. [28]. Based on a DNS analysis over a
189 range of Reynolds numbers [29], it has been reported that the mean value scales with the inverse
190 of the Kolmogorov time scale and can be approximated as $S_{sgs} = 0.28\tau_K^{-1}$. In the current work,
191 the sgs strain rate is estimated from the inverse of the sgs velocity stretching time as:

192 $$S_{sgs} \approx \tau_{stretch}^{-1} = \frac{\sqrt{\frac{2k_{sgs}}{3}}}{\Delta} \tag{22}$$

193 This approach, which brings some consistency with the employed mixing time scale used for
194 combustion modelling, should be seen as a first step before evaluating what would be the
195 appropriate characteristic strain rate to be used for fire simulations in the future. The variation of
196 T_{ign} as a function of S_{sgs} is presented in Fig. 1(a). Nevertheless, the ignition approach described
197 above cannot be applied everywhere in the computational domain without affecting the primary
198 ignition process (i.e., not suppressing the flame just above the burner). For this reason, a small
199 region surrounding the burner (i.e., inside which $T_{ign} = 0$ K) was defined in each scenario where
200 combustion is allowed to take place without allowing for any flame extinction to occur.

201 Modelling of flame extinction is based on the concept of the critical flame temperature, T_{CFT}. The
202 criterion examines whether a reacting mixture within a cell will have enough energy to raise its
203 temperature above T_{CFT} to sustain combustion and is expressed as [3]:

204 $$\hat{Y}_F\big(h_F(\tilde{T}) + \Delta H_c\big) + \hat{Y}_O h_O(\tilde{T}) + \hat{Y}_D h_D(\tilde{T}) > \hat{Y}_F h_F(T_{CFT}) + \hat{Y}_O h_O(T_{CFT}) + \hat{Y}_D h_D(T_{CFT}) \tag{23}$$

205 where sub-scripts F, O and D denote the fuel, oxidizer (i.e., air) and diluents (i.e., inert gases or
206 products of combustion) present in the reacting mixture. Eq. (23) is evaluated based on the initial
207 composition of the reacting mixture, before any combustion occurs. The reacting mixture
208 represents the portion of the grid cell that can potentially react with its composition defined via the
209 following: $\hat{Y}_F = \min(\tilde{Y}_F, \ \tilde{Y}_O/s)$, $\hat{Y}_O = s\hat{Y}_F$ and $\hat{Y}_D = (\hat{Y}_O/\tilde{Y}_O)(\tilde{Y}_F - \hat{Y}_F + \tilde{Y}_D)$. Based on the
210 formulation of the model, the reacting mixture consists of fuel and oxidizer at stoichiometric

211 conditions with any excess fuel within a cell acting as a diluent while any excess air does not.
212 Therefore, combustion within a cell is likely to occur for a small amount of fuel in excess oxidizer
213 but likely to be suppressed for a small amount of oxidizer in excess fuel. If the inequality is true
214 then combustion proceeds as normal, while if the inequality is false, then the reaction within the
215 computational cell is inhibited during the current time step.

216 The critical flame temperature varies locally in every cell and is calculated as:

217
$$T_{CFT} = \left(\tilde{Y}_{N_2} + \tilde{Y}_{CO_2}\right)T_{CFT,(N_2,CO_2)} + \tilde{Y}_{H_2O}T_{CFT,(H_2O)} \tag{24}$$

218 with the critical flame temperature based on the local inert diluents (i.e., N_2, CO_2, H_2O), taken
219 from Perfectly Stirred Reactor (PSR) simulations for different diluent agents with varying
220 concentrations, given by a power law in the form of $T_{CFT,(N_2,CO_2)} = 1407.4\tau_{mix}^{-0.073}$ and
221 $T_{CFT,(H_2O)} = 1517.8\tau_{mix}^{-0.034}$, respectively [24], where τ_{mix} is in ms. A detailed description of the
222 PaSR simulation is provided in [24]. The T_{CFT} values are bounded between 1450 - 1780 K, values
223 which are common minimum and maximum limits for many hydrocarbon fuels. The variation of
224 $T_{CFT,(N_2,CO_2)}$ and $T_{CFT,(H_2O)}$ as a function of τ_{mix} is presented in Fig. 1(b).
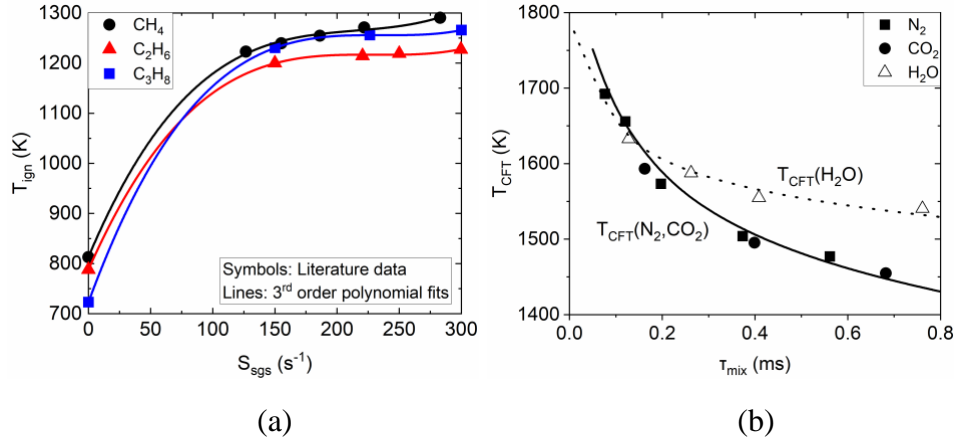
225

226 (a) (b)

227 Fig. 1. Overview of the (a) ignition temperature, T_{ign}, and (b) critical flame temperature, T_{CFT},
228 variation considered in the modelling.

229 It is noted that in our experience in the use of the extinction/(re-)ignition model as implemented
230 and applied for the cases at hand, the ignition model determines the results much more than the
231 extinction model.

232

233 **3. Numerical setup**

234 An overview of the numerical setup used for the numerical simulations of each test case is outlined
235 in Table 2. A local grid refinement strategy is considered so that a fine grid size (i.e., in the order
236 of 1 cm or less) is applied in the near-field region of the fire plumes, and up until the experimentally
237 reported flame heights. The equivalent mass flow rate, accounting for both convective and
238 diffusive mass fluxes, is applied at the burner, while the supply of the co-flowing oxidizer (where
239 present) is provided according to the experiments. The ambient temperature and pressure are 293
240 K and 101325 Pa, respectively, for all scenarios. For angular discretization of the radiative transfer
241 equation 72 solid angles are used, nevertheless the choice of this value is not so influential for

radiative heat transfer inside the flame (not shown here). Second order numerical schemes are used for discretization of the equations. More specifically, a backward scheme is used for time discretization, a filtered linear scheme (i.e., filteredLinear2V) is applied to the convective terms, a TVD scheme (i.e., limitedLinear), which blends central difference and upwind, is employed for scalar transport while a central difference scheme is used for the diffusive terms. The choice of discretization schemes is based on the validation study presented in [30]. A variable time step is employed, limited by a maximum Courant number of 0.9. All simulations without extinction are run for 35 s with averaging occurring over the last 30 s. The extinction cases are run for 90 s, with the oxygen mass fraction in the co-flow remaining constant (i.e., $Y_{O_2} = 0.233$) for the first 4 s and then reduced by 0.002/s [2] (with an equivalent increase in the nitrogen mass fraction, Y_{N_2}).

Table 2. Overview of the setup used in the numerical simulations.

Case	McCaffrey's fire plumes [11]	NIST pool fire [12]	UMD line burner [13]	FM burner[a] [14]
Fuel	CH_4	CH_3OH	CH_4	CH_4, C_2H_4, C_3H_6, C_3H_8,
HRR ($\dot{Q}$)	14.4, 21.7, 33, 44.9, 57.5 kW	256 kW	50 kW	10 - 15 kW
Extinction	No	No	Yes	Yes
Burner	0.3 m x 0.3 m (square)	1 m diameter (circular)	0.5 m x 0.05 m (line)	0.15 m diameter (circular)
Co-flow	-	-	85 g/s	0.041 m/s
Domain	3 m x 3.3 m x 3 m (rectangular)	4 m x 4 m (cylindrical)	1.6 m x 2 m x 1 m (rectangular)	1.2 x 1.8 m (cylindrical)
Grid size (Δ)	1.5 cm (1 m x 2.3 m x 1 m) 3 cm (2 m x 3.3 m x 2 m) 6 cm (domain)	1 cm (1.5 m x 1.5 m) 2 cm (2.5 m x 2.5 m) 4 cm (domain)	0.625 cm (0.6 m x 0.6 m x 0.4 m) 1.25 cm (0.8 m x 0.8 m x 0.6 m) 2.5 cm (domain)	0.5 cm (0.6 m x 0.9 m) 1 cm (0.8 m x 1.2 m) 2 cm (domain)
D^*/Δ	12 - 20	55	-	36
Cells	1.2 million	1.99 million	0.89 million	0.78 million
Rad. fraction ($\chi_{r,exp.}$)[b]	0.17, 0.21, 0.25, 0.27, 0.27	0.21	0.24	0.34

[a] No-extinction cases: C_2H_4 with 15 kW, extinction cases: CH_4, C_2H_4, C_3H_6, C_3H_8 with 10 kW.
[b] Values which are used in Eq. (19) for cases not involving extinction.

4. Results

An overview of the numerical predictions for all the test cases considered (i.e., no-extinction and extinction scenarios) for validation purposes is presented in this section.

4.1 No-extinction cases

Fig. 2 presents a comparison between the CFD predictions and McCaffrey's correlations (i.e., black dashed lines) for the centerline excess temperature and axial velocity. Overall, the simulations on the finest grid size (1.5 cm) exhibit good data clustering, they predict fairly well the maximum temperatures and velocities and they also reproduce the scaling laws suggested by

McCaffrey. Even on a coarser grid (3 cm) the performance of the models is still quite satisfactory for all the heat release rates considered. The predictions on the coarsest grid (6 cm), when only 5 cells are used across the burner, are less satisfactory, which is as expected. Nevertheless, even on such coarse grids the model predictions are still remarkably good for the highest HRR cases (44.9 – 57.5 kW). The numerical predictions for the NIST pool fire and the UMD line burner scenarios, presented in Fig. 3, are also very satisfactory when examining the mean and rms temperatures on the centerline, as well as the radial profiles of temperature at different elevations. Overall, the CFD results are not very grid sensitive and, in most cases, remain close to / within the experimental uncertainty. Equally satisfactory are the simulation results when examining the mean and rms temperatures for the FM burner, shown in Fig. 4. A slightly stronger grid dependency is observed in this case, mainly for the coarsest grid size considered, which is attributed to the lack of sufficient turbulence (i.e., low rms values) above the burner. Any discrepancies in the temperature predictions in this case could also be partially attributed to the combined effect of the absence of soot modelling and the under-prediction of the radiative fractions (i.e., 9% for the 2 cm grid size). Given the strong coupling and dependency between combustion and radiation modelling in fires, these effects are expected to be more important in the FM burner, given its smaller size, compared to the burner sizes involved in the other scenarios. The predicted radiative fractions, χ_r, from all simulations are presented in Table 3. One can observe that the applied correction (i.e., Eq. (19)) in the emission term does result in fairly good and grid insensitive χ_r predictions for all cases and grid sizes when compared to the experimental values (i.e., maximum under-predictions of 12%). The overall satisfactory agreement, even on coarse grid, is due to the dynamic modelling approach.
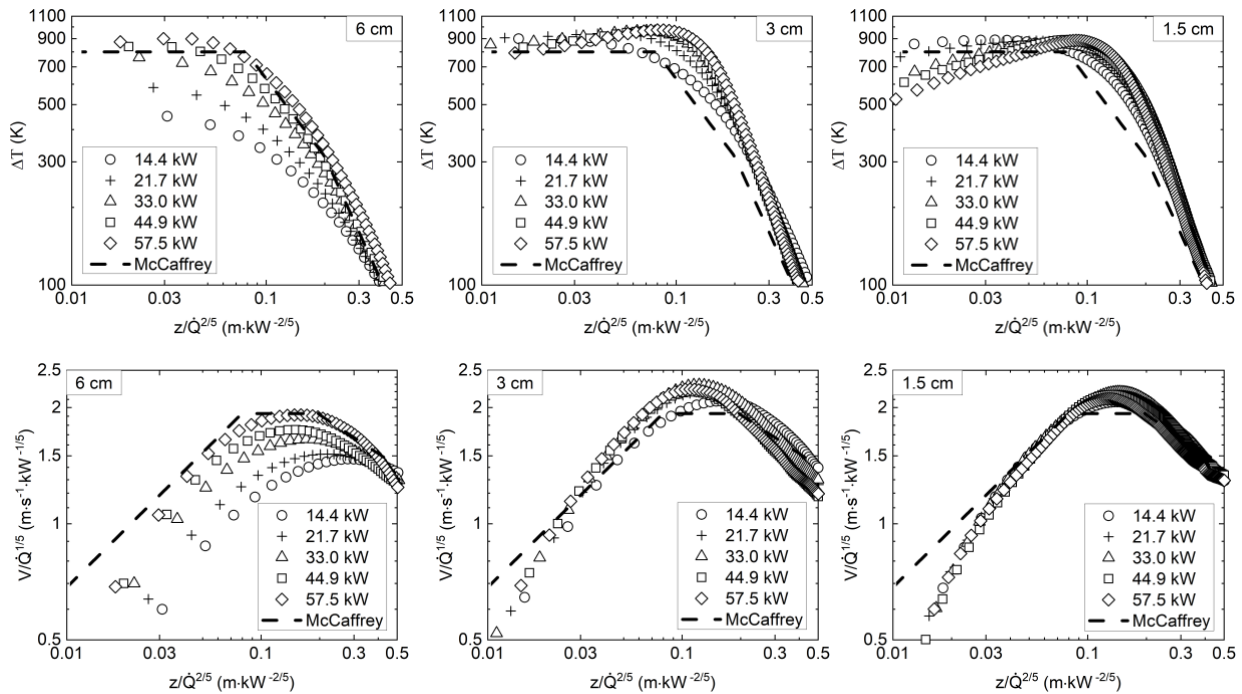

Fig. 2. Centerline mean excess temperature (top) and axial velocity (bottom) for McCaffrey's fire plumes.
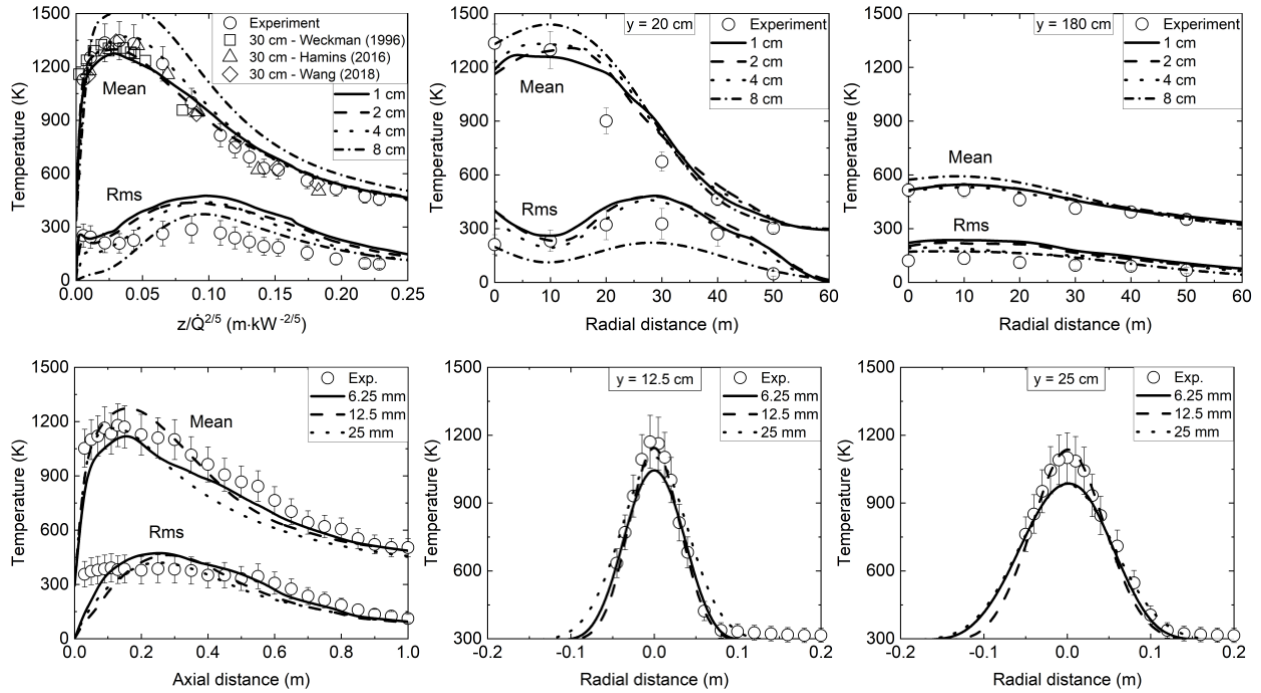
Fig. 3. Temperature on the centerline (left) and at two axial locations (middle, right) for the NIST pool fire (top) and the UMD line burner (bottom).
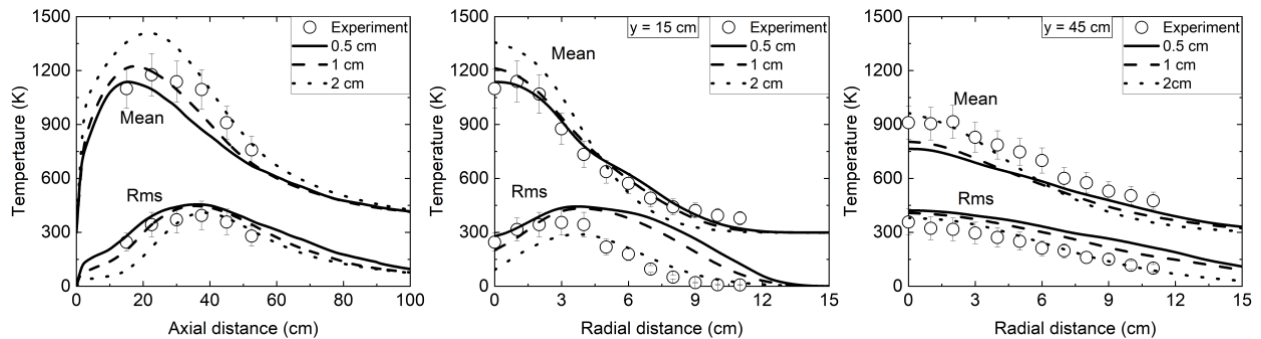

Fig. 4. Temperature on the centerline (left) and at two axial locations (middle, right) for the FM burner.

Table 3. Overview of the predicted radiative fractions, χ_r, in the numerical simulations.

McCaffrey's fire plumes						NIST pool fire 256 kW		UMD line burner 50 kW		FM Burner 15 kW	
	14.4 kW	21.7 kW	33 kW	44.9 kW	57.5 kW						
6 cm	0.15	0.19	0.22	0.24	0.24	4 cm	0.19	2.5 cm	0.21	2 cm	0.31
3 cm	0.15	0.19	0.23	0.24	0.24	2 cm	0.20	1.25 cm	0.22	1 cm	0.32
1.5 cm	0.16	0.19	0.23	0.25	0.25	1 cm	0.20	0.625 cm	0.22	0.5 cm	0.32
Exp.	0.17	0.21	0.25	0.25	0.27	Exp.	0.21	Exp.	0.24	Exp.	0.34

10

4.2 Extinction cases

The predicted combustion efficiencies (i.e., defined as $\eta = \iiint_V \bar{q}_c''' \, dV / \dot{Q}$, where $\dot{Q}$ is the theoretical heat release rate without any flame extinction) are presented in Fig. 5 for the simulations of the UMD line burner and the FM burner with different fuels, as a function of grid size. The predictions with FDS 6.7.8, taken from [31], are also included for comparative purposes. The corresponding limiting oxygen concentrations (LOC) from various sources in the literature are reported in Table 4 and are used, together with the available experimental data, for evaluation of the accuracy and predictive capabilities of the numerical simulations. Emphasis is given on whether the simulations can accurately simulate flame extinction over various grid sizes and whether the predicted LOC values are within the ranges as suggested in the literature.

Table 4. Limiting oxygen concentration (LOC) (vol. %) for different fuel-air-N_2 mixtures.

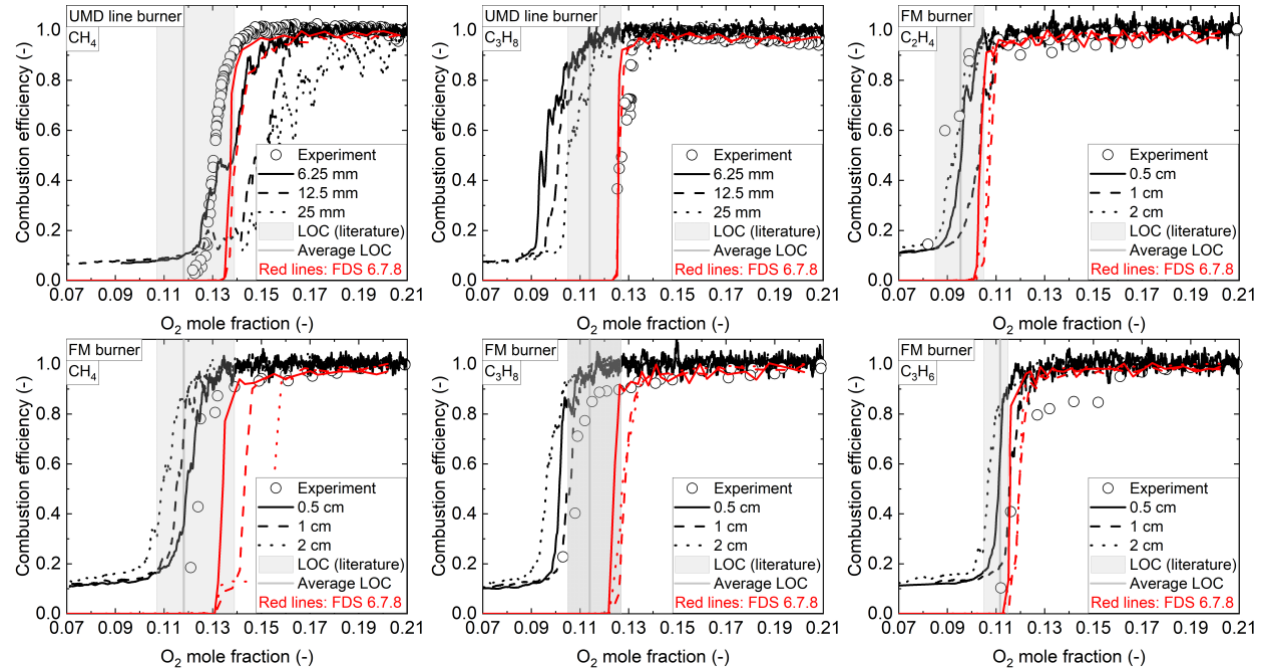| Fuel	Limiting oxygen concentration in % (LOC)
CH_4	10.7 [32], 11.1 [33], 11.3 [34], 11.6 [35], 12 [36, 37], 12.1 [38], 13.9 [39]
C_2H_4	8.5 [33], 8.6 [34], 9.3 [35], 9.9 [36], 10 [37], 10 [38], 10.5 [39]
C_3H_6	10.5 [34], 11.5 [36], 11.5 [38]
C_3H_8	10.5 [34], 10.7 [33], 11.4 [38], 11.5 [37], 11.6 [36], 12.7 [39]

Fig. 5. Predicted combustion efficiency for the different cases and fuels considered.

Overall, the predictions in the FM burner scenario appear to be insensitive to the grid size within the range of Δ values tested (i.e., from 0.5 cm to 2 cm). More specifically, the predictions on the coarsest grid size (i.e., 2 cm) remain acceptable and fairly close to the numerical predictions using the finer grid resolutions (i.e., 1 cm, 0.5 cm). It is worth noting that the LOC value at extinction

323 for a 2 cm grid size tends to be lower compared to the finer grid sizes (i.e., 1 cm, 0.5 cm) due to
324 the slight over-prediction of flame temperatures, previously seen for this scenario without
325 extinction, when the coarsest grid size is employed (i.e., Fig. 4). This aspect is expected to be
326 similar for the simulations with the other fuels as well, even though no comparison is possible due
327 to lack of available experimental data. On the other hand, only the finest of the grid resolutions
328 used in the UMD liner burner scenario (i.e., 6.25 mm) allow to accurately simulate the scenario
329 (i.e., there are 2, 4 and 8 cells across the width of the line burner for a grid size of 25 mm, 12.5
330 mm and 6.25 mm, respectively). This is a consequence of the burner geometry, which is much
331 more demanding in terms of grid resolution. Hence, it is not surprising that a stronger grid
332 dependency is sometimes observed for this scenario (i.e., CH_4 case with a grid size of 25 mm). In
333 addition, it should be emphasized that the reason that all simulations do not tend towards a
334 combustion efficiency of 0 when flame extinction occurs, is due to the small region surrounding
335 the burner where combustion is allowed to take place (i.e., so that the primary ignition source is
336 not affected), as mentioned before.

337 The predicted LOC values from the simulations, using the finest grid sizes, are very satisfactory
338 and usually remain within the range, or close to the lower limit (+- 10%), of the experiments and
339 the values reported in the literature. The only striking difference between the simulations and the
340 experiments appears to be in the UMD liner burner case for C_3H_8. Nevertheless, the predicted
341 LOC values from the simulations are consistent and in the order of 9 – 10%, for both the UMD
342 line burner and the FM burner cases, while the experimental values are different and lie in the
343 order of 12% and 10%, respectively. In this case, the predicted LOC values from the simulations
344 are on the lower end of the values reported in the literature. The general trend for the LOC at
345 extinction in the simulations in the FM burner case is similar to the ones observed in the
346 experiments and with different modelling approaches (e.g., [40]), which is also encouraging with
347 respect to the predictive capabilities of the proposed modelling approach. More specifically, the
348 simulations predict $CH_4(11\%) > C_3H_6, C_3H_8 (10\%) > C_2H_4 (9\%)$ while in the experiments
349 $CH_4(12\%) > C_3H_6(11\%) > C_3H_8 (10\%) > C_2H_4 (8\%)$. Part of the small discrepancies
350 observed for C_3H_6 in the FM burner case (i.e., flame extinction occurring at a slightly lower LOC
351 compared to the experiments) can be attributed to the fact that, in the absence of available
352 experimental T_{ign} data as a function of strain rate and of the radiative fractions as a function of
353 decreasing oxygen concentration, the same input data as in the case of C_3H_8 were used. Similarly,
354 the lack of T_{ign} data for C_2H_4 will also lead to some uncertainty in the flame extinction predictions
355 of these scenarios. Overall, the current numerical results are also in good agreement with the FDS
356 predictions for all scenarios considered, apart from C_3H_8, for which different LOC values at
357 extinction are predicted (i.e., 10% in the present work and 12% for FDS). With the dynamic
358 approach employed here, the numerical predictions are fairly grid insensitive and compare well
359 with both the experimental values and data available from the literature as well as against results
360 predicted with other CFD codes.

361 **4.3 Discussion**

362 Flame ignition and extinction modelling, within the context of infinitely fast chemistry, will
363 inevitably be strongly coupled to turbulence, combustion and radiation modelling. In order to
364 examine the sensitivity of the numerical results, the predicted combustion efficiencies, considering
365 a variation of several modelling parameters (related to flame extinction and radiation modelling),
366 are presented in Fig. 6 for the FM burner with C_2H_4 and a grid size of 1 cm. The use of a constant

367 critical flame temperature, $T_{CFT} = 1610$ K (i.e., value for C_2H_4 based on [9]), gave similar
368 predictions with the approach allowing T_{CFT} to vary with the local mixing time scale (i.e., $T_{CFT} = $
369 $f(\tau_{mix})$). Simulations performed with oxygen model fractions of 21%, 16.8% and 15.2% [14] in
370 the co-flow, resulted in maximum T_{CFT} values in the flame region on the order of 1550-1600 K,
371 exhibiting an increasing trend with decreasing oxygen model fraction. Hence, it is not surprising
372 in this case that the different approaches for modelling T_{CFT} gave similar predictions. On the other
373 hand, the influence of ignition modelling was more important. The consideration of a constant T_{ign}
374 value, set to either the auto-ignition temperature (AIT) of C_2H_4 (i.e., 763 K [9]) or to a commonly
375 used value in the literature (i.e., 1000 K [5]) led to discrepancies by under- and over-predicting the
376 LOC values at extinction, respectively. Based on this, the appropriate range of T_{ign} seems to be in
377 the region of 763-1000 K which essentially lies in between the available experimental data in Fig.
378 1 (a). This aspect suggests that the fitting function used for T_{ign} could potentially have an impact
379 and that there is a need for experimental data for ignition temperatures of various fuels at low strain
380 rates in order to have a more accurate variation of T_{ign} at flow conditions that are more
381 representative for fires. Finally, radiation modelling also seems to be important in this case. More
382 specifically, considering a constant correction for the radiative fraction, (i.e., $\chi_{r,exp.}$ is constant in
383 Eq. (19), set to the value without any flame extinction, and does not decrease as the flame
384 approaches extinction) results in flame extinction occurring much faster than desired. This is to be
385 expected as the flame is forced to lose more heat due to radiation and it approaches extinction
386 faster. Not enforcing any correction on χ_r, results in predictions that agree very well with the
387 experiments. However, this is only by coincidence and due to compensating effects. More
388 specifically, the predicted radiative fraction was initially only 15%, which decreased as a function
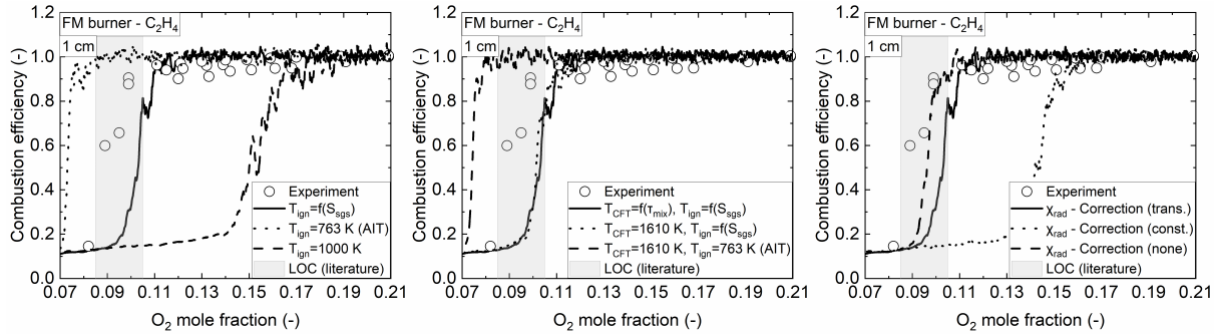389 of time, a value much lower compared to the experimental value of 34%.

390

391 Fig. 6. Sensitivity study on T_{ign} (left), T_{CFT} (middle), and χ_{rad} (right) on the predicted
392 combustion efficiency in the FM burner for C_2H_4 with a grid size of 1 cm.

393 **5. Conclusions**

394 LES results, focusing on flame ignition and extinction modelling, have been presented using a
395 dynamic approach with respect to turbulence, combustion and radiation. Flame ignition was
396 modelled considering an ignition temperature, that varies with the local sgs strain rate, while flame
397 extinction was modelled based on the concept of a critical flame temperature, varying locally with
398 the mixing time scale. As implemented and applied for the cases at hand, the ignition model
399 determined the results much more than the extinction model. Validation of this dynamic approach
400 on four different experiments was made involving both non-extinction and extinction scenarios.

Overall, the numerical simulations were able to accurately predict the reduction in the combustion efficiency of different fuels when the oxygen content in the co-flowing air was reduced. The predicted limiting oxygen concentrations (LOC) values were fairly grid insensitive, as long as a sufficient number of cells were used across the burner and were close to the available experimental data and within the reported range of LOC values reported in the literature ($\pm 10\%$). Both radiation and ignition modelling were reported to be potentially important in this respect. The employed approach showed great potential in terms of modelling flame ignition and extinction using a predictive approach, even on relatively coarse grids. Nevertheless, further validation and refinement of the approach is needed in the future.

Acknowledgements

References

[1] Z. Hu, Y. Utiskul, J.G. Quintiere, A. Trouvé, Towards large eddy simulations of flame extinction and carbon monoxide emission in compartment fires, Proc. Combust. Inst. 31 (2007) 2537-2545. https://doi.org/10.1016/j.proci.2006.08.053

[2] J.P. White, S. Vilfayeau, A.W. Marshall, A. Trouvé, R.J. McDermott, Modeling flame extinction and reignition in large eddy simulations with fast chemistry, Fire Saf. J., 90 (2017) 72-85. https://doi.org/10.1016/j.firesaf.2017.04.023

[3] J. Vaari, J. Floyd, R. McDermott, CFD Simulations on Extinction of Co-Flow Diffusion Flames, Fire Saf. Sci. 10 (2011) 781-793. 10.3801/IAFSS.FSS.10-781

[4] P. Narayanan, H.R. Baum, A. Trouvé, Effect of soot addition on extinction limits of luminous laminar counterflow diffusion flames, Proc. Combust. Inst. 33 (2011) 2539-2546. https://doi.org/10.1016/j.proci.2010.07.003

[5] S. Vilfayeau, N. Ren, Y. Wang, A. Trouvé, Numerical simulation of under ventilated liquid-fueled compartment fires with flame extinction and thermally-driven fuel evaporation, Proc. Combust. Inst. 35 (3) (2015) 2563-2571. https://doi.org/10.1016/j.proci.2014.05.072

[6] S. Vilfayeau, J.P. White, P.B. Sunderland, A.W. Marshall, A. Trouvé, Large eddy simulation of flame extinction in a turbulent line fire exposed to air-nitrogen coflow, Fire Saf. J. 86 (2016) 16-31. https://doi.org/10.1016/j.firesaf.2016.09.003

[7] A.Y. Snegirev, A.S. Tsoy, Treatment of local extinction in CFD fire modeling, Proc. Combust. Inst. 35 (2015) 2519-2526. https://doi.org/10.1016/j.proci.2014.07.051

[8] A.Y. Snegirev, Perfectly stirred reactor model to evaluate extinction of diffusion flame, Combust. Flame 162 (2015) 3622-3631. https://doi.org/10.1016/j.combustflame.2015.06.019

[9] C. Beyler, SFPE Handbook of Fire Protection Engineering, chapter Flammability Limits of Premixed and Diffusion Flames, Springer, New York, 5th edition, 2016.

[10] A. Brown, M. Bruns, M. Gollner, J. Hewson, G. Maragkos, A. Marshall, R. McDermott, B. Merci, T. Rogaume, S. Stoliarov, J. Torero, A. Trouvé, Y. Wang, E. Weckman, Proceedings of the

first workshop organized by the IAFSS Working Group on Measurement and Computation of Fire Phenomena (MaCFP), Fire Saf. J. 101 (2018) 1-17. https://doi.org/10.1016/j.firesaf.2018.08.009

[11] B.J. McCaffrey, Purely Buoyant Diffusion Flames: Some Experimental Results, National Bureau of Standards, NBSIR 79-1910, 1979. https://doi.org/10.6028/nbs.ir.79-1910

[12] K. Sung, J. Chen, M. Bundy, A. Hamins, The characteristics of a 1 m methanol pool fire, Fire Saf. J. 120 (2021) 103121. https://doi.org/10.1016/j.firesaf.2020.103121

[13] J.P. White, E.D. Link, A.C. Trouvé, P.B. Sunderland, A.W. Marshall, J.A. Sheffel, M.L. Corn, M.B. Colket, M. Chaos, H.-Z Yu., Radiative emissions measurements from a buoyant, turbulent line flame under oxidizer-dilution quenching conditions, Fire Saf. J. 76 (2015) 74-84. https://doi.org/10.1016/j.firesaf.2015.05.003

[14] D. Zeng, P. Chatterjee, Y. Wang, The effect of oxygen depletion on soot and thermal radiation in buoyant turbulent diffusion flames, Proc. Combustion Inst. 37 (2019) 825-832. https://doi.org/10.1016/j.proci.2018.05.139

[15] G. Maragkos, B. Merci, On the use of dynamic turbulence modelling in fire applications, Combust. Flame 216 (2020) 9-23. https://doi.org/10.1016/j.combustflame.2020.02.012

[16] P. Moin, K. Squires, W. Cabot, S. Lee, A dynamic subgrid-scale model for compressible turbulence and scalar transport, Phys. Fluids A 3 (1991) 2746-2757. https://doi.org/10.1063/1.858164

[17] C. Fureby, G. Tabor, Mathematical and Physical Constraints on Large-Eddy Simulations, Theoret. Comput. Fluid Dyn. 9 (1997) 85-102. https://doi.org/10.1007/s001620050034

[18] C.C. Nelson, Simulations of spatially evolving compressible turbulence using a local dynamic subgrid model, Ph.D. Thesis, Georgia Institute of Technology, 1997.

[19] B.F. Magnussen, B.H. Hjertager, On Mathematical Modeling of Turbulent Combustion with Special Emphasis on Soot Formation and Combustion, Proc. Comb. Inst. 16 (1977) 719-729. https://doi.org/10.1016/S0082-0784(77)80366-4

[20] V. Sabelnikov, C. Fureby, LES combustion modeling for high Re flames using a multi-phase analogy, Combust. Flame 160 (2013) 83-96. https://doi.org/10.1016/j.combustflame.2012.09.008

[21] G. Maragkos, B. Merci, A fully dynamic approach for turbulence and combustion modelling: Systematic assessment study on fire plumes with variable heat release rate, 12th Mediterranean Combustion Symposium, 23-26 Jan. 2023, Luxor, Egypt.

[22] H.C. Hottel, A.F. Sarofim, Radiative Transfer, McGraw-Hill, New York, 1967.

[23] L.J. Dorigon, G. Duciak, R. Brittes, F. Cassol, M. Galarca, F.H.R. Franca, WSGG Correlations Based on HITEMP2010 for Computation of Thermal Radiation in Non-Isothermal, Non-Homogeneous H2O/CO2 Mixtures, Int. J. Heat Mass Transf. 64 (2013) 863-873. https://doi.org/10.1016/j.ijheatmasstransfer.2013.05.010

[24] V. Sankaran, H. Jiang, M. Colket, S. Zhang, M. Corn, Flame Extinction Model for Fire Suppression Simulations, 9th U.S. National Combustion Meeting, Cincinnati, May 17-20, 2015.

[25] J.C. Hewson, A.R. Kerstein, Local extinction and reignition in nonpremixed turbulent CO/H2/N2 jet flames, Combust. Sci. Technol. 174 (2002) 35-66. https://doi.org/10.1080/713713031

[26] C.G Fotache, H Wang, C.K Law, Ignition of ethane, propane, and butane in counterflow jets of cold fuel versus hot air under variable pressures, Combust. Flame 117 (1999) 777-794. https://doi.org/10.1016/S0010-2180(98)00134-5

[27] C.G. Fotache, T.G. Kreutz, C.K. Law, Ignition of hydrogen-enriched methane by heated air, Combust. Flame 110 (1997) 429-440. https://doi.org/10.1016/S0010-2180(97)00084-9

[28] H-Z Yu, N. Ren, A methodology for applying the counterflow flame extinction propensity to the flame extinction determination in fire simulations, Fire Saf. J. 120 (2021) 103100. https://doi.org/10.1016/j.firesaf.2020.103100

[29] P.K. Yeung, S.S. Girimaji, S.B. Pope, Straining and scalar dissipation on material surfaces in turbulence: Implications for flamelets, Combust. Flame 79 (1990) 340-365. https://doi.org/10.1016/0010-2180(90)90145-H

[30] G. Maragkos, S. Verma, A. Trouvé, B. Merci, Evaluation of OpenFOAM's discretization schemes used for the convective terms in the context of fire simulations, Comput. Fluids 232 (2022) 105208. https://doi.org/10.1016/j.compfluid.2021.105208

[31] K. McGrattan, S. Hostikka, J. Floyd, R. McDermott, M. Vanella, Fire Dynamics Simulator Technical Reference Guide Volume 3: Validation, NIST Special Publication 1018-3, Sixth Edition, 2022. http://dx.doi.org/10.6028/NIST.SP.1018

[32] I.A. Zlochower, G.M. Green, The limiting oxygen concentration and flammability limits of gases and gas mixtures, J. Loss Prev. Process Ind. 22 (2009) 499-505. https://doi.org/10.1016/j.jlp.2009.03.006

[33] K.L. Cashdollar, I.A. Zlochower, G.M Green, R.A Thomas, M. Hertzberg, Flammability of methane, propane, and hydrogen gases, J. Loss Prev. Process Ind. 13 (2000) 327-340. https://doi.org/10.1016/S0950-4230(99)00037-6

[34] S. Kondo, K. Takizawa, A. Takahashi, K. Tokuhashi, A. Sekiya, A study on flammability limits of fuel mixtures, J. Hazard. Mater. 155 (2008) 440-448. https://doi.org/10.1016/j.jhazmat.2007.11.085

[35] C.V. Mashuga, D.A. Crowl, Flammability zone prediction using calculated adiabatic flame temperatures, Proc. Safety Progr. 18 (1999) 127-134. https://doi.org/10.1002/prs.680180303

[36] M. Zabetakis, Flammability Characteristics of Combustible Gases and Vapors, U.S. Bureau of Mines Bull. No. 627, 1965. https://doi.org/10.2172/7328370

[37] J.M. Kuchta, Investigation of fire and explosion accidents in the chemical, mining, and fuel-related industries – a manual, U.S. Bureau of Mines Bulletin, 1985.

[38] H.F. Coward, G.W. Jones, Limits of flammability of gases and vapors, U.S. Bureau of Mines, Bulletin 503, Washington, USA, 1952.

[39] A. Maček, Flammability Limits: A Re-examination, Combust. Sci. Technol. 21 (1979) 43-52. DOI:10.1080/00102207908946917

515 [40] N. Ren, D. Zeng, K.V. Meredith, Y. Wang, S.B. Dorofeev, Modeling of flame extinction/re-
516 ignition in oxygen-reduced environments, Proc. Combustion Inst. 37 (2019) 3951-3958.
517 https://doi.org/10.1016/j.proci.2018.06.076
518

519 **Figure caption list**

520 • Fig. 1. Overview of the (a) ignition temperature, T_{ign}, and (b) critical flame temperature,
521 T_{CFT}, variation considered in the modelling.

522 • Fig. 2. Centerline mean excess temperature (top) and axial velocity (bottom) for
523 McCaffrey's fire plumes.

524 • Fig. 3. Temperature on the centerline (left) and at two axial locations (middle, right) for
525 the NIST pool fire (top) and the UMD line burner (bottom).

526 • Fig. 4. Temperature on the centerline (left) and at two axial locations (middle, right) for
527 the FM burner.

528 • Fig. 5. Predicted combustion efficiency for the different cases and fuels considered.

529 • Fig. 6. Sensitivity study on T_{CFT} (left), T_{ign} (middle) and χ_{rad} (right) on the predicted
530 combustion efficiency in the FM burner for C_2H_4 with a grid size of 1 cm.